Available online at www.sciencedirect.com
SCIENCE DIRECT®
Journal of Organometallic Chemistry 691 (2006) 208–223
Journal of Organometallic Chemistry
www.elsevier.com/locate/jorganchem

Insertion of the p-complex structure of silylenoid H_2SiLiF into X–H bonds (X = C, Si, N, P, O, S, and F)

Ju Xie, Dacheng Feng *, Shengyu Feng

Institute of Theoretical Chemistry, School of Chemistry and Chemical Engineering, Shandong University, Jinan 250100, PR China

Received 2 March 2005; received in revised form 13 August 2005; accepted 23 August 2005
Available online 4 October 2005

Abstract

The insertion reactions of the p-complex structure (A) of silylenoid H_2SiLiF into XH_n molecules (X = C, Si, N, P, O, S, and F; $n = 1$–4) have been studied by ab initio calculations at the G3(MP2) level. The results indicate that the insertion reactions of A into X–H bonds proceed via three reaction paths, I, II, and III, forming the same products, substituted silanes H_3SiXH_{n-1} with dissociation of LiF, respectively, and all insertion reactions are exothermic. All the seven X–H bonds can undergo insertion reactions with A via path I and II, but only four of them, C–H, Si–H, P–H, and S–H, undergo insertion reactions via path III. The following conclusions emerge from this work: (i) the X–H insertion reactions of A occur in a concerted manner via a three-membered ring transition state; (ii) for path I and II, the stabilization energies of the A–XH_n complexes decrease in the order $HF > H_2O > H_2S > NH_3 > SiH_4 > CH_4$; (iii) for path I and II, the greater the atomic number of heteroatom (X) in a given row, the easier the insertion reaction of XH_n hydrides and the larger the exothermicity, and for the second-row hydrides, the reaction barriers are lower than for the first-row hydrides; (iv) The barriers of path I are lowest in those of three pathways with the exception of A + SiH_4 system, which barrier of path III is lowest. Moreover, the present study demonstrates that both electronic and steric effects play major roles in the course of insertion reactions of A into X–H bonds.

Keywords: Silylenoid H_2SiLiF; p-Complex structure; Insertion reactions; G3(MP2) theory

1. Introduction

Early in the 1960s, silylenoids, analogues to carbenoids, were postulated as intermediates in some organosilicon reactions [1,2]. For example, in the reduction of dichlorodialkylsilanes R_2SiCl_2 with alkali metals M to synthesize polysilanes, the reaction process was supposed experimentally as following:

$$R_2SiCl_2 + M \xrightarrow{-MCl} \underset{\text{silylenoid}}{R_2SiMCl} \xrightarrow{-MCl} \underset{\text{silylene}}{R_2Si} \longrightarrow \underset{\text{polysilane}}{-(R_2Si)_n-}$$

Since then people tried to detect, even to obtain some silylenoid species as well as to probe into their structures and properties [3–11]. However, as a kind of very reactive species, the preparation of silylenoids is very difficult. Until 1995, Tamao et al. [12] reported the first experimental study of silylenoid chemistry, detected the existence of [(*tert*-butoxy)diphenylsilyl]lithium, $Ph_2SiLi(OBu\text{-}t)$, and investigated its chemical properties. In 1998, Tanake et al. [13] studied the self-condensation reaction of lithium (alkoxy)silylenoid as a model of $Ph_2SiLi(OBu\text{-}t)$ using ab initio method. In 2004, Lee et al. [14] reported the syntheses of stable halosilylenoids $(Tsi)X_2SiLi$ ($Tsi = C(SiMe_3)_3$; X = Br, Cl) at room temperature. Thus, a great breakthrough has been experimentally made in the research of silylenoids. The theoretical studies on silylenoids were lagged. In 1980, Clark et al. [15] studied theoretically the isomers of lithoflurosilylenoid H_2SiLiF by ab initio calculations for the first time. Since 1990s, we have studied some silylenoids such as R_1R_2SiMX (R_1,R_2 = H, F, OH, NH_2, Me, Et; X = F, Cl, Br; M = Li, Na, K, etc.) by

* Corresponding author. Tel.: +86 0531 88365748; fax.: +86 0531 88564464.
E-mail addresses: xieju@sdu.edu.cn (J. Xie), fdc@sdu.edu.cn (D. Feng).

0022-328X/$ - see front matter © 2005 Elsevier B.V. All rights reserved.
doi:10.1016/j.jorganchem.2005.08.031

quantum chemistry theory on their structures, stability, isomerization, insertion reactions, and addition reactions etc [16–20]. Recently [21], we theoretically studied the structures and isomerization of silylenoid $Ph_2SiLi(OBu\text{-}t)$, and found its three-membered ring (a) and the p-complex (b) structures more stable than the other isomers, which is well consistent with the experimental presuming [12]. Both experimental and theoretical results show that silylenoids have ambiphilic character, nucleophilicity and electrophilicity, and can take part in many reactions. Such reactions as insertion, addition, and polymerization were recognized as important and effective methods for preparation of the new silicon-bonded and heterocyclic silicon compounds. Therefore, further thorough investigations on silylenoids will be of important theoretical and practical values.

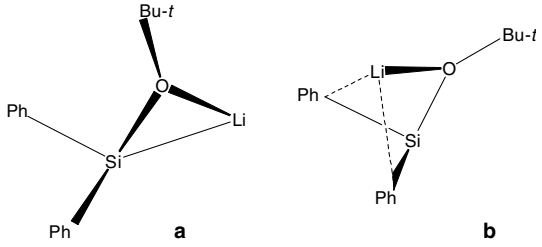

However, for insertion reactions, one of the important reactions of silylenoids, the theoretical studies are rare. The only two theoretical studies [16,18] on the insertion reactions of H_2SiLiF and $H_2SiLiCl$ into H_2 molecule were performed, respectively, by our group. In this paper, we have undertaken a systematic investigation of the insertion reactions (1) of the p-complex structure (A) of silylenoid H_2SiLiF, the simplest model compound, into first- and second-row hydrides XH_n (where X is a p-block element) using G3(MP2) theory.

$$H_2SiLiF + H\text{–}XH_{n-1} \rightarrow H_3SiXH_{n-1} + LiF \qquad (1)$$
$$X = C, Si, N, P, O, S, F; \quad n = 4, 4, 3, 3, 2, 2, 1$$

Through this theoretical work, we hope (i) to clarify the reaction mechanism and to determine the structures and energetics of all stationary points, (ii) to investigate the thermodynamics of structure A insertion reactions with CH_4, SiH_4, NH_3, PH_3, H_2O, H_2S, and HF molecules, (iii) to estimate their activation barriers and to understand the origin of the barrier heights, and (iv) to establish general trends and predictions for the insertion of silylenoid into X–H bonds.

2. Computational methods

The geometries and frequencies of all stationary points (reactants, precursor complexes, transition states, intermediates and products) were firstly optimized at the HF/6-31g(d) level. All structures were then reoptimized at MP2(full)/6-31G(d) level, followed by single-point calculations carried out at QCISD(t,fc)/6-31G(d)//MP2(full)/6-31G(d) and MP2(fc)/G3(MP2)large//MP2(full)/6-31G(d) levels, respectively. Finally, G3(MP2) theory [22] was used for calculations of structural energies. The minimum energy paths (MEP) were obtained by the intrinsic reaction coordinate (IRC) [23,24] calculations with a gradient step size of 0.05 $(amu)^{1/2}$ bohr at the MP2(full)/6-31G(d) level. In addition, natural bond orbital (NBO) [25] analyses at the MP2(full)/6-31G(d) level were used to demonstrate the charge-transfer during the insertion reactions. The GAUSSIAN 03 series of programs were employed in all calculations [26].

3. Results and discussion

The previous calculations [15,17,19,21] show that each of silylenoids R_2SiMX has four equilibrium isomers, the three-membered ring, the p-complex (four-membered ring), the σ-complex (linear), and the "classical" tetrahedral structures. It is indicated that the three-membered ring and the p-complex structures are the two most stable and experimentally detectable ones in chemical reactions. The p-complex structure A (see Fig. 1) of silylenoid H_2SiLiF is adopted in the present study. Structure A can be considered as a silylene complex with ionic compound LiF. The singlet silylene H_2Si (see Fig. 1) has C_{2v} symmetry, and has both nucleophilicity in σ orbital (HOMO) direction and electrophilicity in the p orbital (LUMO) direction. Structure A with C_s symmetry is formed by electron donating of F atom in compound LiF toward unoccupied p orbital of Si atom in H_2Si. In fact there also exists weak interaction among the positive Li atom and two negative H atoms. This means that there are two "loose" four-membered rings, H–Si–F–Li–H, which make A stable, and its G3(MP2) energy is even 17.63 kJ/mol lower than that of the three-membered ring structure. As shown in Fig. 1, the main part of HOMO in A is the σ orbital on Si atom (occupancy number: 1.988), and the main part of LUMO is localized on Li atom (occupancy number: 0.036). In addition, the σ orbital on Si atom is exposed, and there exists enough space under the Si atom, where the insertion

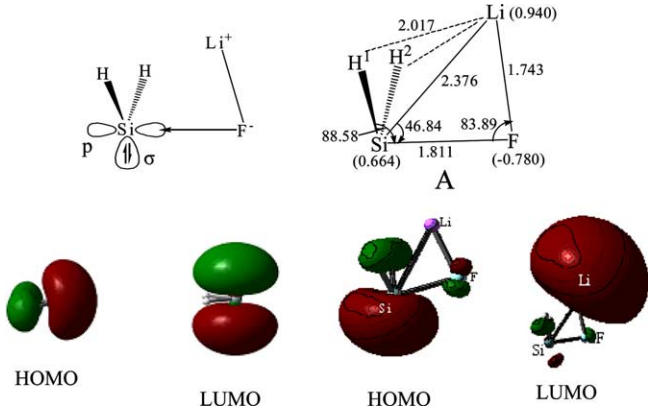

Fig. 1. The HOMO and LUMO of H_2Si and p-complex structure (A) of H_2SiLiF, and the structure and natural charges (in parentheses) for atoms of A (bond lengths, Å; bond angles, °) at MP2(full)/6-31g(d) level.

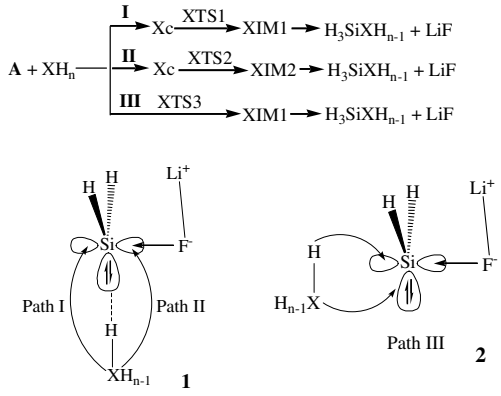

Scheme 1. Three reaction paths, I, II, and III, for the insertion reactions of A into X–H bonds.

reactions of A into X–H bonds take place (see Scheme 1 (1), path I and II). Moreover, it is intriguing to note that there exists the third insertion pathway (see Scheme 1 (2), path III) for insertion reactions of A into C–H, Si–H, P–H, and S–H bonds.

3.1. Path I

3.1.1. Precursor complexes

It is reasonable to expect that the first step in the A reaction with small molecules is the formation of a precursor complex (Xc). The calculated geometries of the precursor complexes (Cc, Sic, Nc, Oc, Sc, and Fc) are depicted in Fig. 2, respectively. The total energies for reactants ($XH_n + A$) and relative energies for other structures (relative to the corresponding reactants) are given in Table 1.

Several interesting conclusions can be drawn from these figures and the table. As can be seen in Fig. 2, these precursor complexes, Cc, Nc, Oc, Sc, and Fc, appear to have the same structure, in which the positive H end of X–H bond interacts on the σ orbital on Si atom (see Scheme 1 (1)). For these precursor complexes, the Si–H distance increases in the order Fc (2.507 Å) < Oc (2.858 Å) < Sc (3.069 Å) < Nc (3.243 Å) < Cc (3.641 Å). The stability energy (relative to the corresponding reactants) decreases in the order Fc (26.67 kJ/mol) > Oc (12.68 kJ/mol) > Sc (8.13 kJ/mol) > Nc (4.77 kJ/mol) > Cc (1.44 kJ/mol). These trends of the precursor complexes can be explained by the nature of the XH_n hydride and that of structure A, and by steric effect. The natural charges of H atom in hydrides HF, H_2O, NH_3, CH_4, and H_2S molecules are 0.560, 0.480, 0.372, 0.217, and 0.133, respectively. Therefore structure A should form much more stable complexes with HF and H_2O than with NH_3, CH_4, H_2S. In addition, the steric effect also plays an important role in forming the precursor complexes, because XH_3 or XH_4 molecules couldn't get close to Si atom in structure A easily. This leads to a longer Si–H distance and a smaller value for the stability energy.

In the case of SiH_4, its precursor complex (Sic, see Fig. 2) displays a different $LiFH_2Si\cdots SiH_4$ bonding characteristics. That is, SiH_4 molecule interacts on σ orbital on Si atom in A mainly via the electropositive Si atom in SiH_4 instead of H atom. There exist three loose three-membered ring, Si–H–Si, in Sic, which make it more stable than Cc by 3.31 kJ/mol, although Si···Si (4.268 Å) and Si···H distances (4.00 Å or so) are very long. Electronegativity of P element is almost same as that of H element, and the natural charge of P atom in PH_3 is only 0.124. It is difficult that PH_3 molecule interacts on σ orbital on Si atom in A directly. Our attempt to locate the precursor complex of PH_3 and A failed.

There is little variation in the structural parameters of H_2SiLiF and XH_n moieties in Xc, relative to the corresponding reactants A and XH_n. However, it can be found from natural bond orbital (NBO) analyses that the transfer of σ electrons of Si atom in A to XH_n moiety does occur. Compared with the occupancy number (1.988) of σ orbital on Si atom in A, that of σ orbital on Si atom in Xc increases in the order Fc (1.948) < Oc (1.975) < Sc (1.977) < Sic (1.981) < Nc (1.984) < Cc (1.987). Accordingly, the natural charge of XH_nmoiety in Xc increases in the order HF (−0.0458) < H_2O (−0.0153) < H_2S (−0.0125) < SiH_4 (−0.0082) < NH_3 (−0.0045) < CH_4 (−0.0021). Thus, our theoretical findings suggest that A shows nucleophilic behaviour in the process from the beginning of the insertion to precursor complex.

3.1.2. Transition states

As XH_n further approaches A, the XH_{n-1} group moves toward and interacts with the p orbital on Si atom from the back-side of the F atom in A (see Scheme 1 (1)). Then transition state XTS1 reached. The optimized transition states along with the calculated natural charges on selected atoms are given in Fig. 2 (the hydrogen in X–H bonds, fluorin in HF molecule, and silicon in SiH_4 molecule marked as H*, F*, and Si*, respectively). The relative energies (relative to the corresponding reactants) are given in Table 1.

All transition states at the MP2(full)/6-31 g(d) level are confirmed by calculation of the energy Hessian which shows only one imaginary vibrational frequency. It should be mentioned that the primary similarity among those transition states is the three-center pattern involving silicon, hydrogen H*, and heteroatoms X.

One of the interesting points to emerge from calculations of XTS1 geometries is the extent to which Si–H* and Si–X bonds are formed in the transition state. Relative to their values in the product (vide infra), the Si–H* and Si–X bond lengths in CTS1, NTS1, OTS1, and FTS1 are (1.5%, 23.1%), (8.8%, 16.1%), (7.4%, 24.3%), and (9.0%, 30.5%) longer than those in the corresponding products, respectively. Additionally, the distance of the X–H* bond to be broken is 48.9%, 36.9%, 38.1%, and 30.3% longer than that of the corresponding reactant XH_n for X = C, N, O, and F, respectively. All these features indicate that the F–H and O–H insertion reactions arrive at the transition states relatively early, whereas the C–H and N–H insertion reactions reach the transition states relatively late. In other words, this indicates that the closer the X atom is

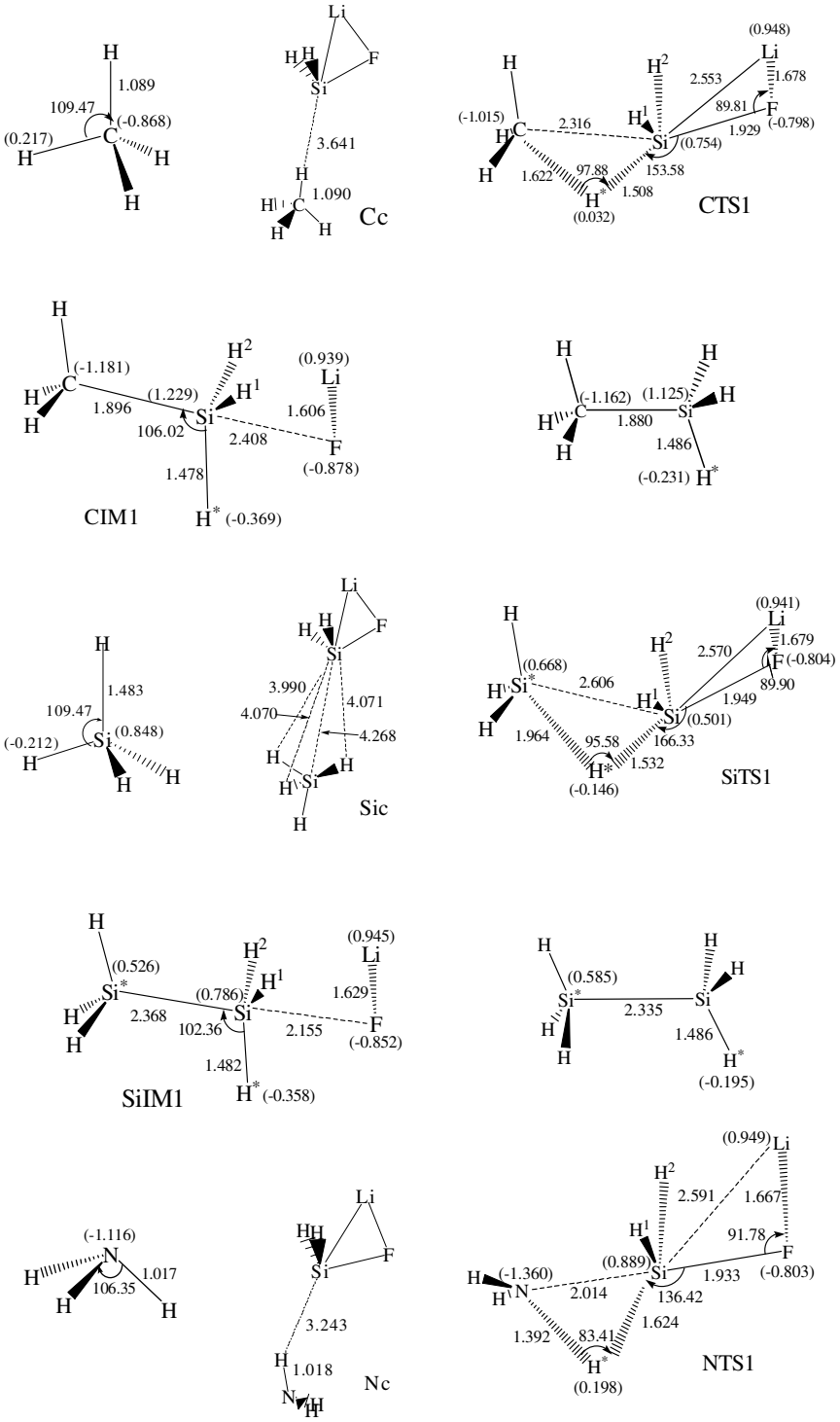

Fig. 2. Optimized geometries (bond lengths, Å; bond angles, °) and natural charges for atoms (in parentheses) of transition states (XTS1), intermediates (XIM1) and products for path I at MP2(full)/6-31g(d) level.

to the end of a period, the earlier the transition state is formed. These observations will be related to the predicted energetics below.

We now consider the barriers for structure A insertion into the first- and second-row hydrides. As can be seen from Table 1 and Fig. 2, one may obtain two main results: (a) the activation barrier decreases in the order $CH_4 > NH_3 > H_2O > HF$ and $SiH_4 > PH_3 > H_2S$, and (b) the barrier heights for the first-row hydrides are much higher than those for the second-row hydrides, i.e., $CH_4 > SiH_4$, $NH_3 > PH_3$, and $H_2O > H_2S$. For instance, the G3(MP2) calculations estimate that the energies of CTS1, NTS1, OTS1, and FTS1 are above those of the reactants by 208.17, 157.87, 117.43, and 74.06 kJ/mol and the activation energies from

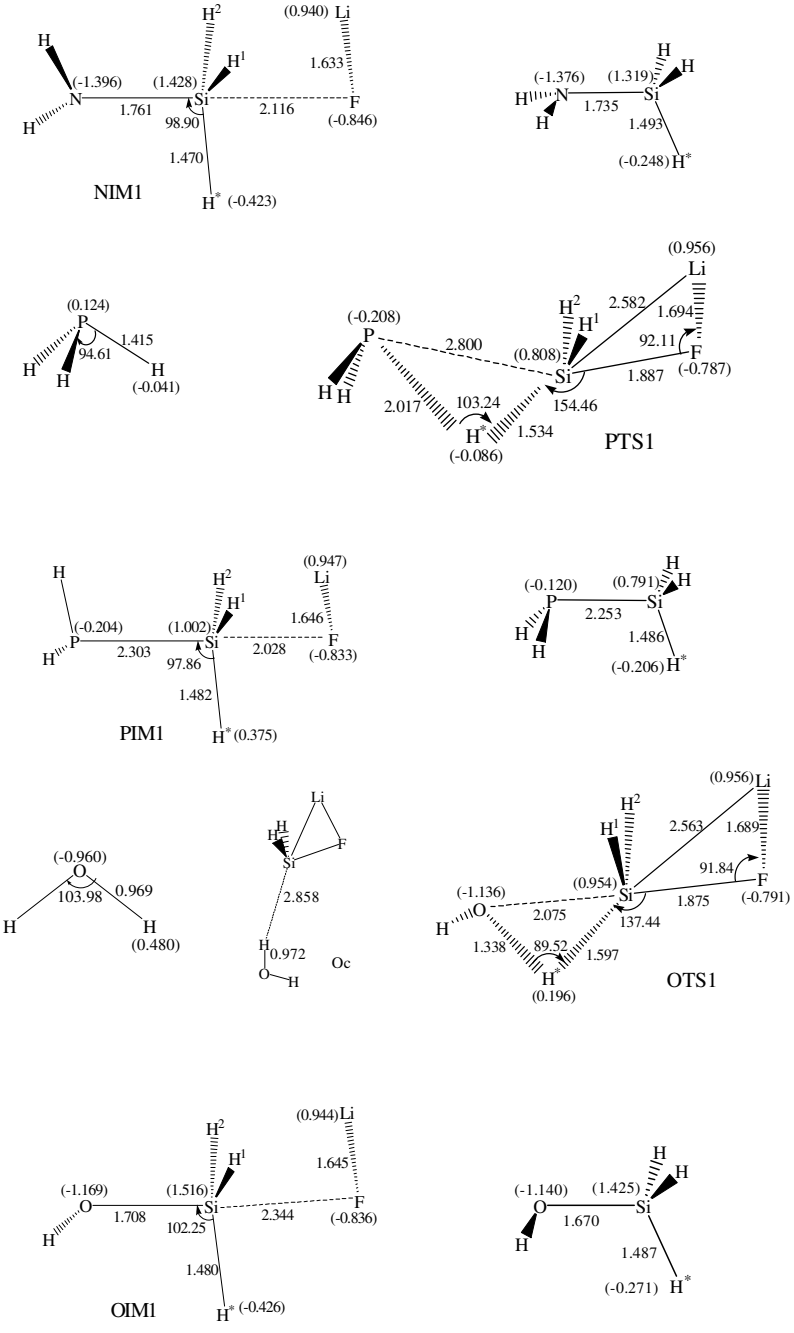

Fig. 2 (*continued*)

the corresponding precursor complex are 209.61, 162.64, 130.11, and 100.73 kJ/mol, respectively. Also, the G3(MP2) calculations suggest that the energies of SiTS1, PTS1, and STS1 are above those of the reactants by 103.49, 86.06, and 63.11 kJ/mol and the activation energies for the overall reaction are 108.24, 86.06, and 71.24 kJ/mol, respectively. On this basis, one may therefore conclude that the A insertion reaction with XH (X = F), and XH_2 (X = O, S) is essentially more favorable than that with XH_4 (X = C, Si) and XH_3 (X = N, P). In addition, the model calculations also suggest that X–H insertions for the second-row hydrides occur more readily than those for the first-row hydrides. Consequently, our theoretical results are in complete accord with the Hammond postulate [27], which associates a reactant-like transition state with a smaller barrier and a more exothermic reaction (vide infra).

The explanation for the activation barrier trends is connected with the nature of the XH_n hydride and that of A, and with steric effects. Electronegativity of X element and hydrogen is in the order: F > O > N > C ≈ S > H ≈ P > Si. As shown in Scheme 1(1), it is easier for the high-lying σ orbital and the low-lying p orbital on Si atom to interact with H–F bond than with C–H bond. This interaction results in a lower barrier height for HF insertion. On the other hand, it is relatively difficult for A to approach CH_4 molecule and a higher barrier for this reaction than

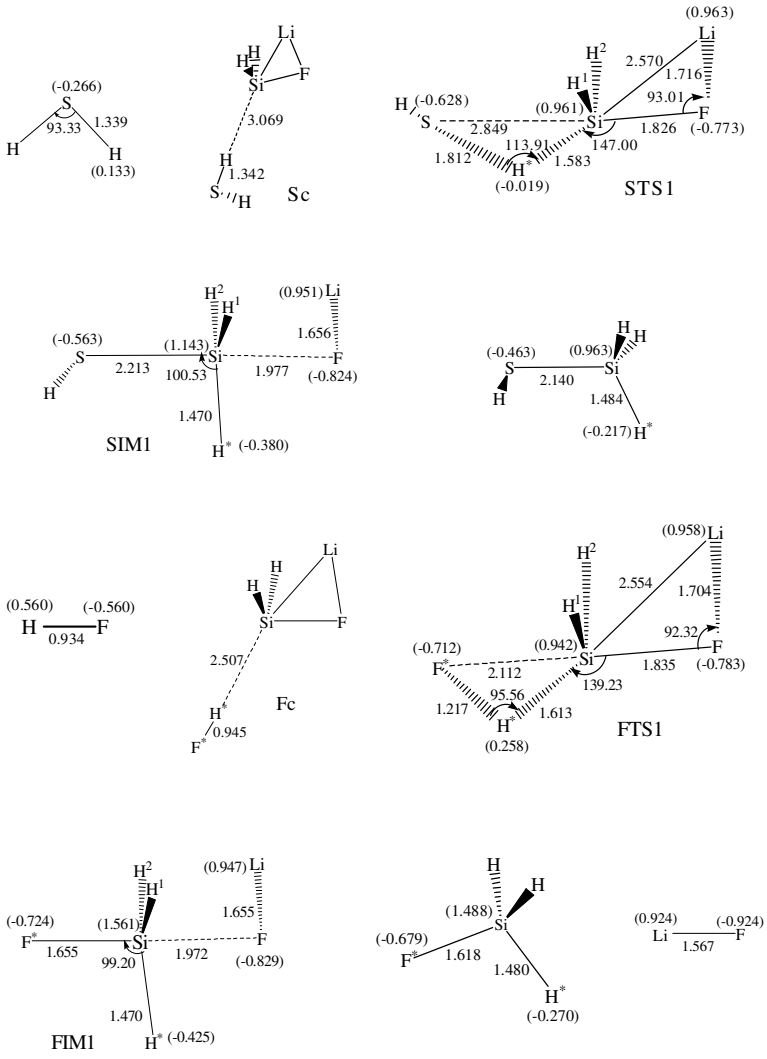

Fig. 2 (*continued*)

the other XH_n hydride reaction is therefore expected. In other words, the greater the atomic number of heteroatom (X) in a given row, the easier the insertion reaction of XH_n hydrides. For the same family systems, the steric factor is minor and the X–H bond strengths may come to play a dominant role. The X–H bond strength for the first-row hydride is bigger that that for the corresponding second-row hydride. Namely, the C–H bond is more difficult to activate than the Si–H bond. Therefore, the X–H insertion for the second-row hydrides has a lower activation barrier than that for the first-row hydrides.

To get more specific information on this subject, NBO analysis has been performed at MP2(full)/6-31g(d) level, which correlates well with changes in bond lengths and it provides characteristics that are closely connected to basic chemical concepts. As can be seen from Fig. 2, the varieties of electric charges of atoms and groups are obvious. The natural charges of Si atom in H_2SiLiF moiety increased in the order CTS1 (0.754) < NTS1 (0.889) < FTS1 (0.942) < OTS1 (0.954) and <SiTS1 (0.501) < PTS1 (0.808) < STS1 (0.961) relative to that of Si atom in A (0.664). The natural charges of H^*XH_{n-1} moiety in XTS1 decreased in the order CH_4 (−0.332) > NH_3 (−0.375) > HF (−0.453) > H_2O (−.469) and SiH_4 (0.121) > PH_3 (−0.396) > H_2S (−0.540). The occupancies of Si–H* and Si–X bonds to be formed in CTS1, NTS1, SiTS1, PTS1, and STS1 are (1.796, 1.895), (1.910, 1.956), (1.836, 1.844), (1.840, 1.905), and (1.735, 1.892), respectively. Additionally, in OTS1 and FTS1, the Si–H* bond has formed with occupancy 1.979 and 1.944, respectively, however the Si–X (X = O and F) interactions are still very weak. This finding is consistent with the prediction above that the F–H and O–H insertion reactions arrive at the transition states relatively early. It is also indicates that the Si–H* bond formed earlier than that of the Si–X bond.

3.1.3. Insertion intermediates

After getting over transition state XTS1, the Si–H* and Si–X bonds formed gradually with rupturing of H*–X bond. The LiF moiety separates away from Si atom with reducing Li–F distance. Then the intermediate XIM1 forms (see Fig. 2). Geometry of XIM1 is similar and

Table 1
The total energies (a.u.) for reactants ($XH_n + A$) and relative energies[a] (kJ/mol) for other structures

Structure	MP2(full)/6-31G(d)	G3(MP2)
A (H_2SiLiF)	−397.290882	−397.539481
LiF	−107.129465	−107.292150
X = C		
$CH_4 + A$	−437.627924 (0.0)	−437.961581 (0.0)
Cc	−2.23	−1.44
CTS1	241.73	208.17
CIM1	−39.99	−49.07
CTS2	290.65	245.69
CIM2	−2.40	−11.36
CTS3	306.63	266.08
$H_3SiCH_3 + LiF$	−5.09	−24.61
X = Si		
$SiH_4 + A$	−688.607732 (0.0)	−688.970133 (0.0)
Sic	−4.92	−4.75
SiTS1	130.87	103.49
SiIM1	−51.23	−48.95
SiTS2	199.45	161.73
SiIM2	−72.42	−70.48
SiTS3	96.22	72.11
$H_3SiSiH_3 + LiF$	−17.96	−28.32
X = N		
$NH_3 + A$	−453.648260 (0.0)	−454.009622 (0.0)
Nc	−9.71	−4.77
NTS1	170.09	157.87
NIM1	−114.13	−108.82
NTS2	198.18	181.54
NIM2	−79.80	−71.73
$H_3SiNH_2 + LiF$	−62.69	−73.13
X = P		
$PH_3 + A$	−739.853141 (0.0)	−740.231648 (0.0)
PTS1	117.23	86.06
PIM1	−84.29	−75.10
PTS2	158.88	118.74
PIM2	−92.35	−78.93
PTS3	158.65	127.30
$H_3SiPH_2 + LiF$	−36.67	−44.96
X = O		
$H_2O + A$	−473.490126 (0.0)	−473.881889 (0.0)
Oc	−17.38	−12.68
OTS1	110.43	117.43
OIM1	−178.11	−154.87
OTS2	138.22	137.37
$H_3SiOH + LiF$	−113.22	−111.03
X = S		
$H_2S + A$	−796.089580 (0.0)	−796.483809 (0.0)
Sc	−10.03	−8.13
STS1	84.50	63.11
SIM1	−141.24	−123.03
STS2	104.87	79.69
SIM2	−140.75	−117.77
STS3	207.02	172.21
$H_3SiSH + LiF$	−75.52	−78.59
X = F		
$HF + A$	−497.475043(0.0)	−497.898263(0.0)
Fc	−28.78	−26.67
FTS1	53.52	74.06
FIM1	−260.50	−213.41
FTS2	73.55	88.21
FIM2	−230.82	−188.21
$H_3SiF + LiF$	−177.27	−150.10

[a] Relative to the corresponding reactants.

analogous to a trigonal bipyramidal complex. The X and F atoms are located at two peaks, respectively. The process from transition state to intermediate is also that of inversion of the triangular cone "umbrella" formed by Si atom and three H atoms, and that of X atom reacting with Si from back of F atom with the departing of F from Si. As a whole, this process is similar to S_N2-Si type nucleophilic substitution mechanism [28]. In XIM1, the Si–X distance has greatly shortened to 1.896 Å (CIM1), 1.761 Å (NIM1), 1.708 Å (OIM1), 1.655 Å (FIM1), and 2.368 Å (SiIM1), 2.303 Å (PIM1), 2.213 Å (SIM1), respectively, which is almost equal to that in corresponding product H_3SiXH_{n-1}, respectively. X–Si bond has formed. In addition, the distance between F and Si atoms is about 2.0 Å, and the interaction between them has become very weak. In fact, XIM1 is a complex of silane H_3SiXH_{n-1} with LiF. The G3(MP2) results suggest that the relative energy of XIM1 for the first-row XH_n hydrides decreases in the order CIM1 (−49.07 kJ/mol) > NIM1 (−108.82 kJ/mol) > OIM1 (−154.87 kJ/mol) > FIM1 (−213.41 kJ/mol). Likewise, the relative G3(MP2) energy for the second-row XH_n hydrides is predicted to be in the order SiIM1 (−48.95 kJ/mol) > PIM1 (−75.10 kJ/mol) > SIM1 (−123.03 kJ/mol).

3.1.4. Insertion products

When LiF moiety separates away completely from Si atom, silane H_3SiXH_{n-1} can be obtained. The equilibrium geometries for the insertion products H_3SiXH_{n-1} are presented in Fig. 2, respectively. The reaction enthalpies at G3(MP2) levels of theory are plotted in Fig. 8 together with the reaction enthalpies of the XH*n* hydride systems given in Table 1.

The theoretical results depicted in Figs. 2–8 show that all the insertion products H_3SiXH_{n-1} adopt a tetracoordinate conformation on the silicon center. Furthermore, it is apparent that all the A insertions are thermodynamically exothermic. In fact, from Fig. 8 it can first be noted that there are large similarities in the trends for the first-row and second-row insertion products. There is, for example, a clear trend toward larger reaction enthalpy on moving along a row. Namely, the G3(MP2) results suggest that the reaction enthalpy for the first-row XH_n hydrides decreases in the order CH_4 (−24.61 kJ/mol) > NH_3 (−73.13 kJ/mol) > H_2O (−111.03 kJ/mol) > HF (−150.10 kJ/mol). Likewise, the exothermicity for the second-row XH_n hydrides is predicted to be in the order SiH_4 (−28.32 kJ/mol) > PH_3 (−44.96 kJ/mol) > H_2S (−78.59 kJ/mol). In summary, the periodic trends in the energetics of these seven systems are especially interesting. First, our theoretical findings indicate that for A insertions there is a very clear trend toward lower activation barriers and more exothermic interactions on going from left to right along a given row. Second, for the second-row hydrides, the insertion reactions are less exothermic (with the exception of $A + XH_4$ system) than for the first-row hydrides and the reaction barriers are lower.

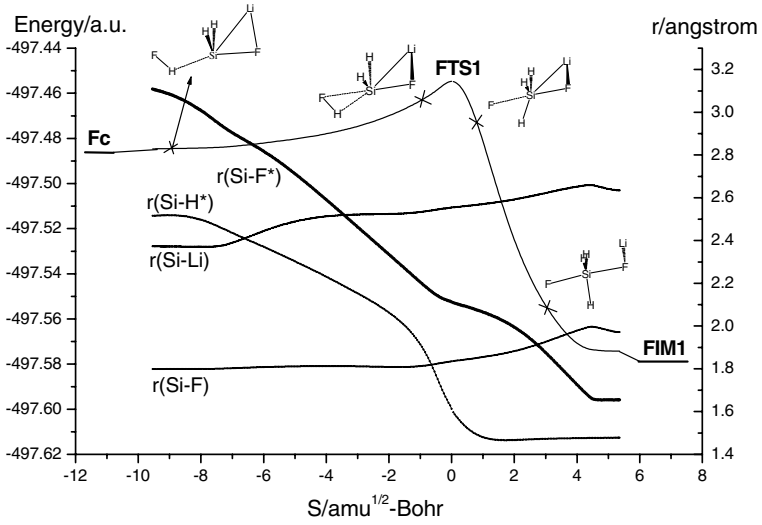

Fig. 3. Energy and bond length vs. reaction coordinate (S) in reaction path I for the insertion of A into HF at MP2(full)/6-31g(d).

3.1.5. Reaction path properties

The intrinsic reaction coordinate (IRC) calculations on $A + XH_n$ (X = C, Si, N, P, O, S, and F; $n = 1$–4) systems have been performed at the MP2(full)/6-31g(d) level. For instance, Fig. 3 shows the energy changes and the variations of Si–F*, Si–H*, Si–F, and Si–Li distances along the reaction coordinate in reaction path for A + HF system. The energies and some geometries selected at −9.62, −1.00, 1.00, and 2.50 $(amu)^{1/2}$ bohr along the IRC for HF insertion are also shown in Fig. 3, where it may be seen that the transition state FTS1 connects smoothly with both the precursor complex Fc and the insertion intermediate FIM1. NBO analysis along this IRC for selected points is given in Table 2. It is obvious that the bond lengths, Si–H* and Si–F*, change strongly in the course of reaction. The Si–H* bond rapidly shortens from reactants side and arrives at the equilibrium bond length of FIM1 at about $s = 1.00\ (amu)^{1/2}$ bohr. The Si–F* bond arrives at the equilibrium bond length of FIM1 at about $s = 4.50\ (amu)^{1/2}$ bohr. It appears that the formation of Si–H* bond is earlier than that of Si–F* bond. In addition, the Si–Li and Si–F bond lengths during the course of reaction elongate gradually to the equilibrium bond lengths of FIM1 at about $s = 4.50\ (amu)^{1/2}$ bohr. In Table 2, it is found that the charges of H_2Si moiety increase during the course of reaction with those of H* and F* decrease, respectively. There is little variation in the charges of LiF moiety. For example, at $s = -9.62$, the charges of H_2Si and H*F* moieties are −0.159 and −0.013, respectively. At $s = -1.00$, those of H_2Si and H*F* moieties are −0.088 and −0.083, respectively. Simultaneously, the occupancies of the lone pair orbital on Si atom (LP_{Si}, σ orbital) decrease from 1.968 ($s = -9.62$) to 1.859 ($s = -1.00$), relative to 1.988 in A. It is indicate that A shows nucleophilic behaviour in the σ orbital direction in the beginning of the insertion. In the region from $s = -0.50$ to 2.50 $(amu)^{1/2}$bohr, the charges of H_2Si moiety have increased from −0.002 ($s = -0.50$) to 0.836 ($s = 2.50$), and the Si–H* and Si–F* bonds formed with the inversion of configuration of F^*SiH_3 moiety. It is reasonable to say that the insertion process involves a S_N2-Si type reaction mechanism [28].

The intermediate FIM1 can further decompose to substituted silane H_3SiF and compound LiF. We investigated the variation of energies for optimized geometries which were obtained by freezing a certain Si–F distance and optimizing the other geometric parameters at MP2(full)/6-31G(d) level. The calculations results are available as supporting information. When LiF separates away completely from Si atom, product H_3SiF can be obtained.

For reactions $A + XH_n$ (X = C, Si, N, P, O, and S; $n = 2$–4), the reaction mechanism are similar to that of A + HF reaction.

3.2. Path II

As can be seen from Scheme 1 that paths I and II share the same precursor complex (Xc, see Fig. 2). As the Si···H distance further shortening, the X atom interacts with the p orbital on Si atom from the front-side of the F atom in A (see Scheme 1 (2)). Namely, the X atom attacks at Si atom from the same side of the LiF moiety, making the reaction proceed via path II. This insertion path involves the initial formation of a precursor complex (Xc, see Fig. 2), followed by an intermediate IM2 via a transition state XTS2, and then the product, substituted silane H_3SiXH_{n-1} and LiF (see Scheme 1). The optimized transition states XTS2 and insertion intermediates XIM2 along with the calculated natural charges on selected atoms are given in Fig. 4 (the hydrogen in H–X bonds, fluorin in HF molecule, and Silicon in SiH_4 molecule marked as H*, F*, and Si*, respectively). The total energies for reactants ($XH_n + A$) and relative energies for other structures (relative to the corresponding reactants) are given in Table 1.

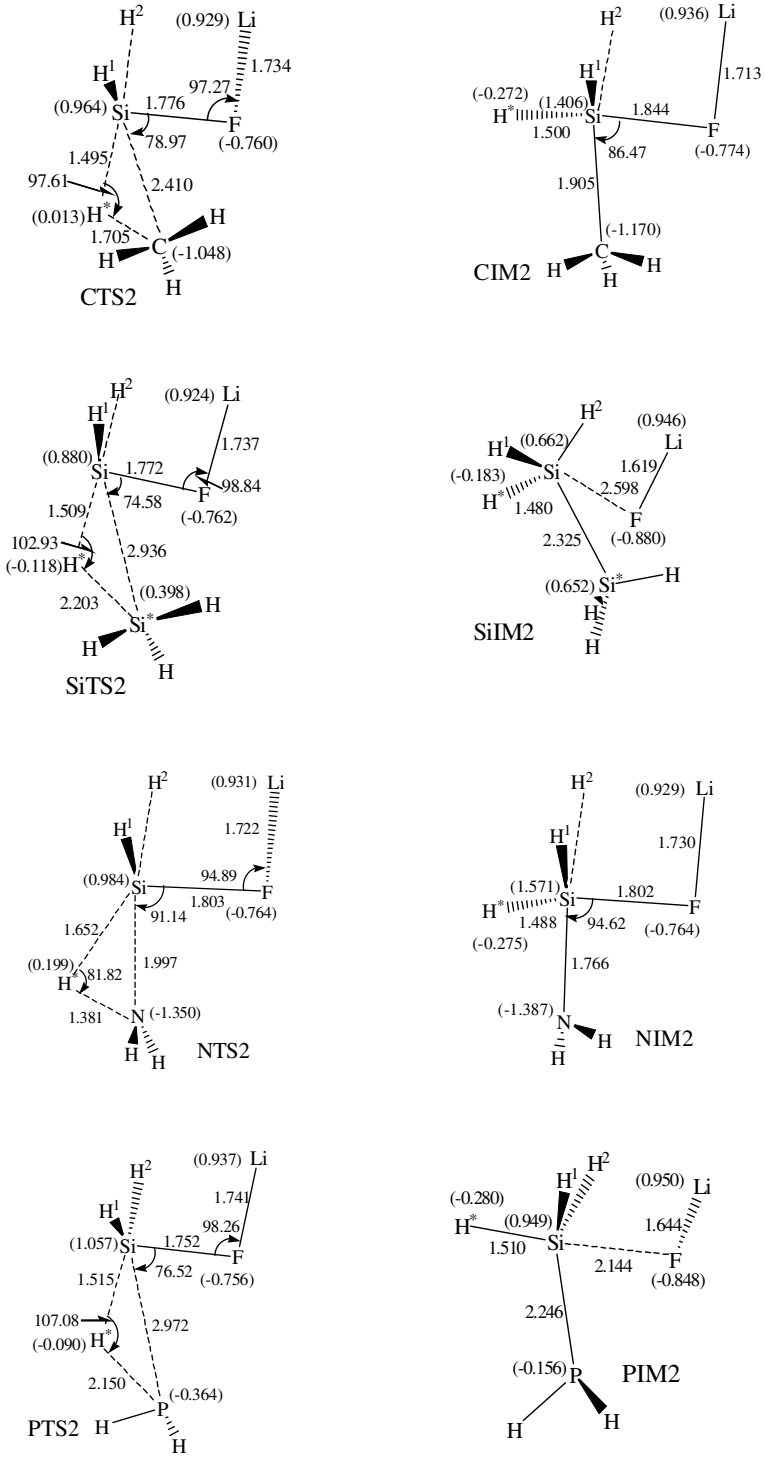

Fig. 4. Optimized geometries (bond lengths, Å; bond angles, °) and natural charges for atoms (in parentheses) of transition states (XTS2) and intermediates (XIM2) for path II at MP2(full)/6-31g(d) level.

3.2.1. Transition states

After the precursor complex Xc, the transition state XTS2 was found for path II of the insertion reactions of A into X–H bonds. Geometry of seven XTS2 is similar and involves a Si–H*–X three-membered ring structure (see Fig. 4). The Si–H* and Si–X bond lengths in CTS2, NTS2, OTS2, FTS2, and SiTS2, PTS2, STS2 are (0.6%, 28.2%), (10.6%, 15.1%), (7.9%, 24.3%), (8.4%, 31.3%), and (1.5%, 25.7%), (2.0%, 31.9%), (4.4%, 41.5%) longer than those in the corresponding products H_3SiXH_{n-1} (see Fig. 2), respectively. Also, the breaking X–H* bond is stretched by 56.6%, 35.8%, 38.6%, 32.2%, and 48.6%, 51.9%, 45.1% relative to its equilibrium value in XH_n as X changes from C to N to O to F and from Si to P to S,

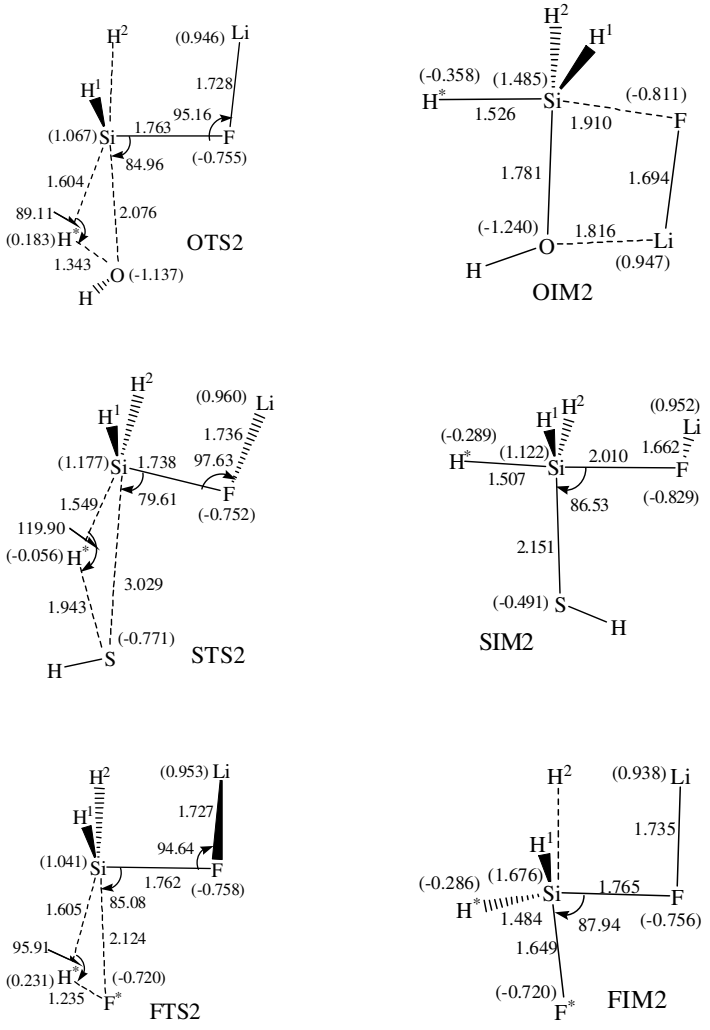

Fig. 4 (*continued*)

respectively. Taken together, these values strongly suggest that the transition state structures for HF and H_2O take on a more reactant-like character than for CH_4 and that for H_2S take on a more reactant-like character than for SiH_4 molecule. On the other hand, as seen in Table 1, it is apparent that the activation barrier decreases in the

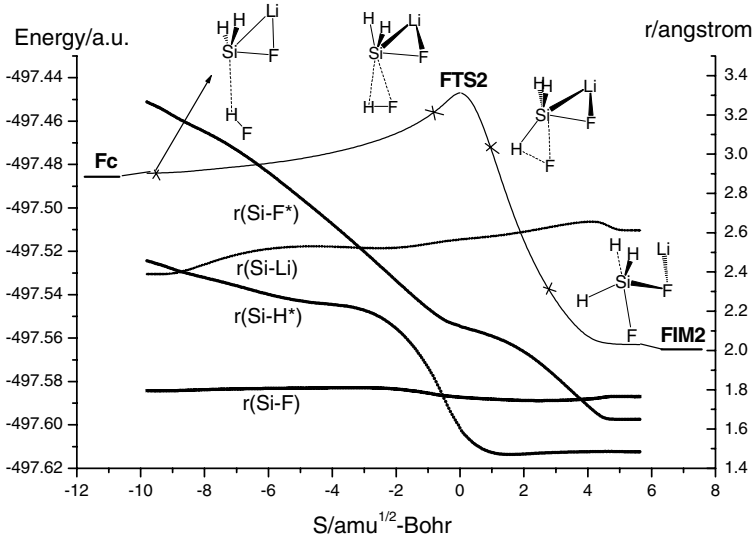

Fig. 5. Energy and bond length vs. reaction coordinate (*S*) in reaction path II for the insertion of A into HF at MP2(full)/6-31g(d).

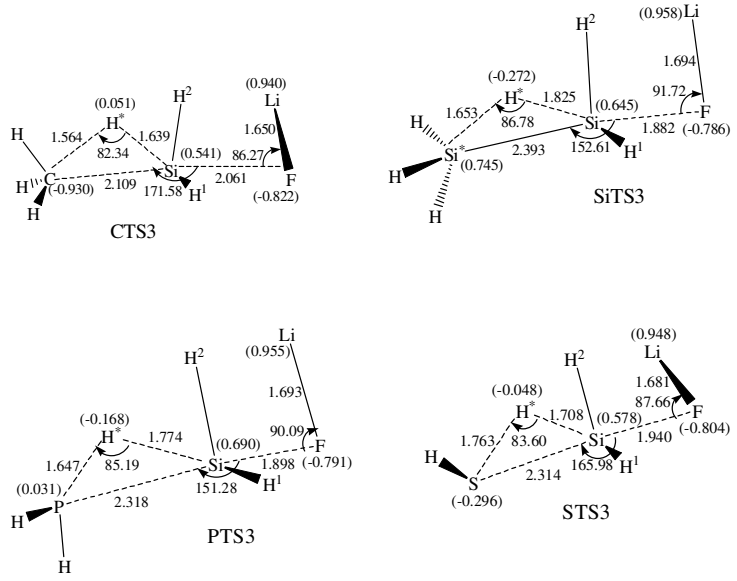

Fig. 6. Optimized geometries (bond lengths, Å; bond angles, °) and natural charges for atoms (in parentheses) of transition states (XTS3) for path III at MP2(full)/6-31g(d) level.

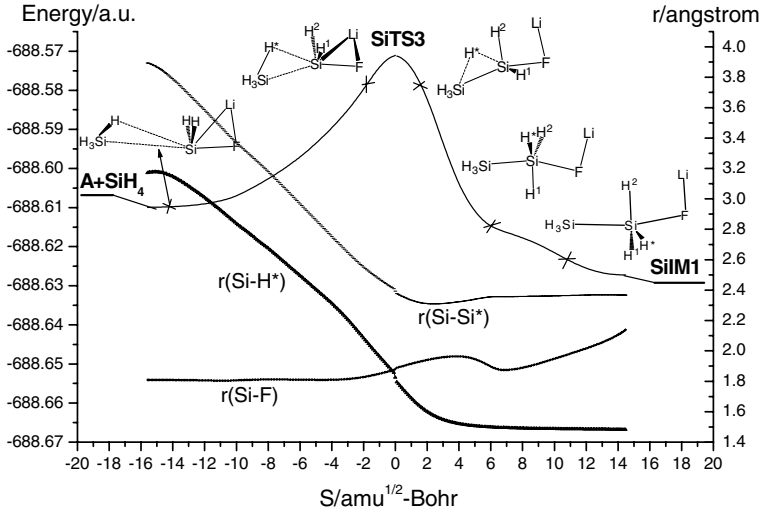

Fig. 7. Energy and bond length vs. reaction coordinate (S) in reaction path III for the insertion of A into SiH_4 at MP2(full)/6-31g(d).

order: CH_4 (247.13 kJ/mol) > NH_3 (186.31 kJ/mol) > H_2O (150.05 kJ/mol) > HF (114.88 kJ/mol) and SiH_4 (166.48 kJ/mol) > PH_3 (118.74 kJ/mol) > H_2S (87.82 kJ/mol). This is consistent with the Hammond postulate [27]. In addition, the barrier heights for the first-row hydrides are much higher than those for the second-row hydrides.

The natural charges of Si atom in H_2SiLiF moiety increased in the order CTS2 (0.964) < NTS2 (0.984) < FTS2 (1.041) < OTS2 (1.067) and <SiTS2 (0.880) < PTS2 (1.057) < STS2 (1.177) relative to that of Si atom in A (0.664). The natural charges of H^*XH_{n-1} moiety in XTS2 decreased in the order NH_3 (−0.357) > CH_4 (−0.419) > H_2O (−0.488) ≈ HF (−0.489) and SiH_4 (−0.386) > PH_3 (−0.579) > H_2S (−0.727). The occupancies of Si–H* and Si–X bonds to be formed in CTS2, NTS2, SiTS2, and PTS2 are (1.839, 1.865), (1.763, 1.950), (1.889, 1.809), and (1.870, 1.870), respectively. Additionally, in STS2, OTS2 and FTS2, the Si–H* bond has formed with occupancy 1.971, 1.946 and 1.949, respectively, however the Si···X (X = S, O and F) interactions are still very weak. This finding is consistent with the prediction above that the S–H, O–H and F–H insertion reactions arrive at the transition state relatively early.

3.2.2. Insertion intermediates

After getting over transition state, Si–H* and Si–X bonds are formed gradually. Simultaneously, H*–X bond broke,

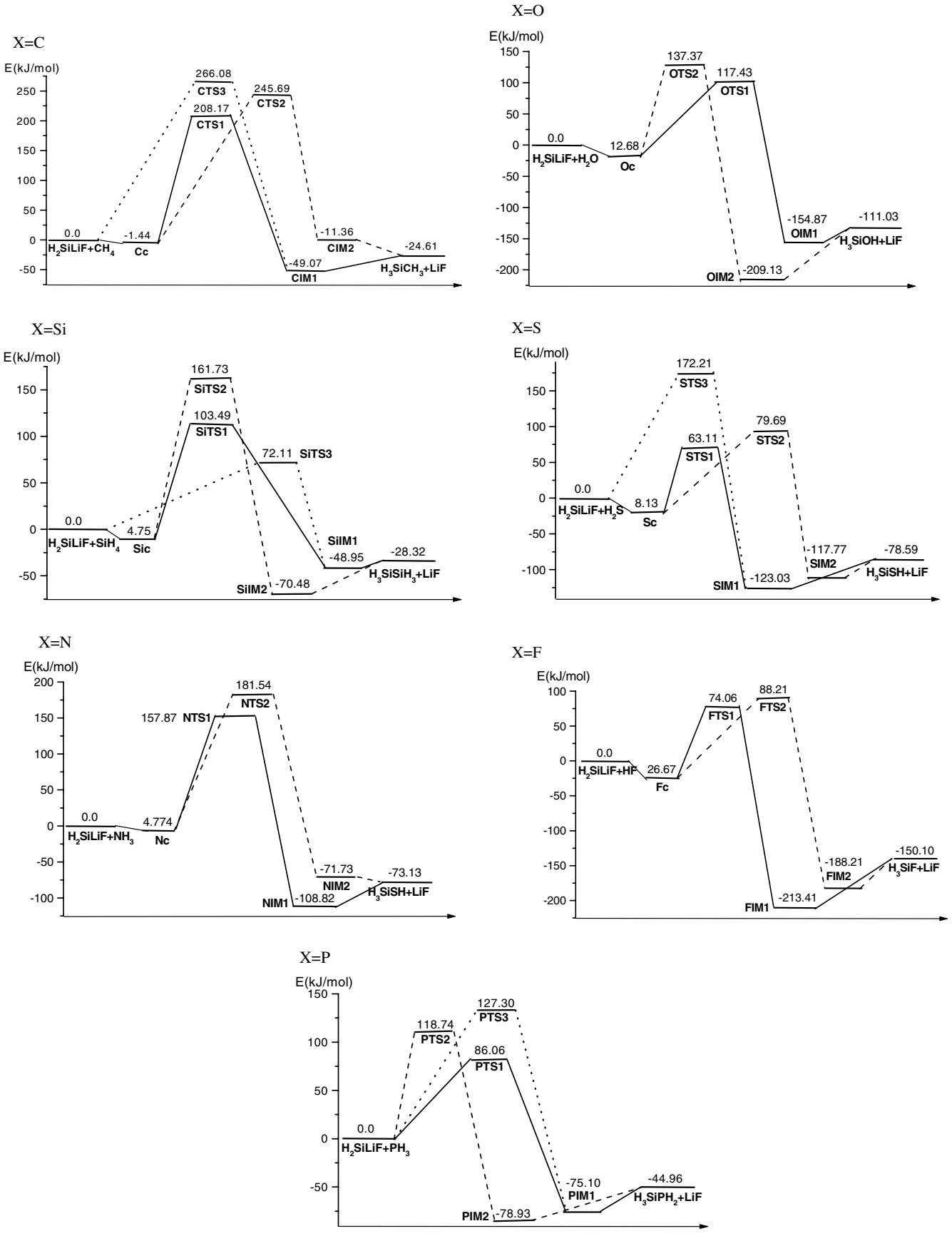

Fig. 8. The schematic diagram of the potential energy curves at G3(MP2) level.

Table 2
Natural bond orbital analyses along MP2(full)/6-31g(d) IRCs for reactions A + HF (path I), A + HF (path II), and A + SiH_4 (path III)

s/(amu)$^{1/2}$	Charges for atoms or groups					Bond occupancy			Occupancy	
	H_2Si	F	Li	H*	X	Si–F	Si–H*	Si–X	LP_{Si}	LP^*_{Si}
A + HF reaction of path I, X = F*										
−9.62	−0.159	−0.775	0.948	0.571	−0.584	1.993			1.968	
−1.00	−0.088	−0.784	0.955	0.539	−0.622				1.859	0.184
−0.50	−0.002	−0.785	0.956	0.477	−0.647	1.991	1.925			
0.00	0.279	−0.783	0.958	0.258	−0.712	1.990	1.944			
1.00	0.713	−0.786	0.956	−0.095	−0.788	1.955	1.942	1.964		
2.50	0.836	−0.808	0.954	−0.232	−0.749	1.963	1.917	1.953		
A + HF reaction of path II, X = F*										
−9.80	−0.147	−0.773	0.951	0.562	−0.592	1.993			1.958	0.185
−1.00	−0.098	−0.768	0.947	0.537	−0.619				1.859	
−0.50	−0.004	−0.764	0.948	0.464	−0.649	1.992	1.921			
0.00	0.294	−0.758	0.953	0.231	−0.720	1.992	1.949			
1.00	0.704	−0.752	0.958	−0.119	−0.791	1.969	1.943	1.962		
2.50	0.800	−0.753	0.951	−0.253	−0.745	1.969	1.922	1.950		
A + SiH_4 reaction of path III, X = Si*										
−14.75	−0.158	−0.779	0.943	−0.221	0.215	1.993			1.981	
−1.49	−0.021	−0.779	0.959	−0.235	0.075				1.700	0.269
−0.99	−0.005	−0.781	0.959	−0.243	0.070				1.659	0.293
−0.49	0.013	−0.783	0.959	−0.253	0.064				1.610	0.322
0.00	0.048	−0.786	0.958	−0.272	0.052		1.692	1.681		
1.49	0.117	−0.796	0.952	−0.303	0.030		1.845	1.931		
5.99	0.163	−0.788	0.943	−0.245	−0.074		1.979	1.943		

and <H*SiX increased. Insertion intermediates XIM2 formed (see Fig. 4), respectively. XIM2 can be regarded as a complex of H_3SiXH_{n-1} with LiF. The Si–X distance has greatly shortened to 1.905 Å (CIM2), 1.766 Å (NIM2), 1.781 Å (OIM2), 1.649 Å (FIM2), and 2.325 Å (SiIM2), 2.246 Å (PIM2), 2.151 Å (SIM2), respectively, which is almost equal to that in corresponding product H_3SiXH_{n-1}, respectively. The G3(MP2) results suggest that the relative energy of XIM2 for the first-row XH_n hydrides decreases in the order CIM2 (−11.36 kJ/mol) > NIM2 (−71.73 kJ/mol) > FIM2 (−188.21 kJ/mol) > OIM2 (−209.13 kJ/mol). Likewise, the relative G3(MP2) energy for the second-row XH_n hydrides is predicted to be in the order SiIM2 (−70.48 kJ/mol) > PIM2 (−78.93 kJ/mol) > SIM2 (−117.77 kJ/mol).

3.2.3. Reaction path properties

The intrinsic reaction coordinate (IRC) calculations on A + XH_n (X = C, Si, N, P, O, S, and F; n = 1–4) systems have been performed at the MP2(full)/6-31g(d) level. For instance, Fig. 5 shows the energy changes and the variations of Si–F*, Si–H*, Si–F, and Si–Li distances along the reaction coordinate in reaction path for A + HF system. The energies and some geometries selected at −9.80, −1.00, 1.00, and 2.50 (amu)$^{1/2}$ bohr along the IRC for HF insertion are also shown in Fig. 5, where it may be seen that the transition state FTS2 connects smoothly with both the precursor complex Fc and the insertion intermediate FIM2. NBO analysis along this IRC for selected points is given in Table 2. It is obvious that the bond lengths, Si–H* and Si–F*, change strongly in the course of reaction. The Si–H* bond rapidly shortens from reactants side and arrives at the equilibrium bond length of FIM2 at about s = 1.00 (amu)$^{1/2}$ bohr. The Si–F* bond arrives at the equilibrium bond length of FIM2 at about s = 4.50 (amu)$^{1/2}$ bohr. It appears that the formation of Si–H* bond is earlier than that of Si–F* bond. In addition, the Si–Li bond length during the course of reaction elongates gradually to the equilibrium bond length of FIM2 at about s = 4.50 (amu)$^{1/2}$ bohr, and the change of the Si–F bong length becomes slow. Similar to path I, it can be seen from Table 2 (path II), it is found that the charges of H_2Si moiety increase during the course of reaction with those of H* and F* decrease, respectively. It is also indicate that A shows nucleophilic behaviour in the insertion. In the region from s = −0.50 to 2.50 (amu)$^{1/2}$bohr, the Si–H* and Si–F* bonds formed with the retention of configuration of F*SiH_3 moiety. It is reasonable to say that the insertion process is similar to a S_Ni-Si type reaction mechanism [28].

The intermediate FIM2 can further decompose to substituted silane H_3SiF and compound LiF. For reactions A + XH_n (X = C, Si, N, P, O, and S; n = 2–4), the reaction mechanism are similar to that of A + HF reaction.

3.3. Path III

Different from paths I and II, when molecule XH_n approaches A with the X end of H–X bond attacking the σ orbital of Si atom and the H end approaching the p orbital of Si atom from the back-side of F atom in A, the reaction undergoes according to path III (see Scheme 1 (2)). If the electronegativity of X element is very high in comparison

to that of hydrogen, it is difficult that the electronegative X atom interacts with the high-lying σ orbital (HOMO) on Si atom at the beginning of the insertion reaction. Our theoretical results indicate that A can react only with four kinds of XH_n, CH_4, SiH_4, PH_3, and H_2S, in seven hydrides investigated via path III. This path involves the formation of a transition state XTS3 (see Fig. 6), followed by an intermediate XIM1 leading to the product H_3SiXH_{n-1} with LiF being dissociated apart from the Si atom (see Scheme 1).

3.3.1. Transition states

The calculated geometries of the transition states CTS3, SiTS3, PTS3 and STS3, are shown in Fig. 6 (silicon in SiH_4 and the migratory hydrogen of X–H bond marked as Si* and H*, respectively). The total energies for reactants ($XH_n + A$) and relative energies for other structures (relative to the corresponding reactants) are given in Table 1. Relative to their values in the product H_3SiXH_{n-1} (see Fig. 2), the Si–H* and Si–X bond lengths in CTS3, SiTS3, PTS3, and STS3 are (10.3%, 12.2%), (22.8%, 2.48%), (19.4%, 2.9%), and (15.1%, 8.1%) longer than those in the corresponding products, respectively. The occupancies of Si–H* and Si–X bonds to be formed in CTS3, SiTS3, PTS3, and STS3 are (1.743, 1.767), (1.692, 1.681), (1.675, 1.737), and (1.754, 1.778), respectively. Additionally, the distance of the X–H* bond to be broken is 43.6%, 11.5%, 16.4%, and 31.7% longer than that of the corresponding reactant XH_n for X = C, Si, P, and S, respectively. In four transition states the Si–F bonds elongate to 2.061 Å (CTS3), 1.882 Å (SiTS3), 1.898 Å (PTS3) and 1.940 Å (STS3), respectively. Namely there has existed the tendency of leaving of LiF moiety from Si atom in transition states. All these features indicate that the Si–H insertion reaction arrives at the transition state relatively early, whereas the C–H and S–H insertion reactions reach the transition states relatively late. The activation barriers for four insertion reactions increased in the order: 72.11 kJ/mol (SiTS3) > 127.30 kJ/mol (PTS3) > 172.21 kJ/mol (STS3) > 266.08 kJ/mol (CTS3). Our theoretical findings are consistent with the Hammond postulate [27].

The trend in the barrier height of XTS3 (X = C, Si, P, and S) can be explained by the nature of the XH_n hydride and that of structure A, and by steric effects. Electronegativity of X element and hydrogen is in the order: C ≈ S > H ≈ P > Si. As shown in Scheme 1 (2), it is easier for the high-lying σ orbital on Si atom to interact with the electropositive Si* end of Si–H bond in SiH_4 than with electronegative C or S atoms in CH_4 or H_2S. Likewise, the electronegative H end of Si–H bond in SiH_4 can act on the low-lying p orbital on Si atom in A more favorably. On the other hand, the steric effect also plays an important role in forming the transition states, because CH_4 molecule couldn't get close to Si atom in structure A easily. This leads to a higher activation barrier for $A + CH_4$ system. Therefore path III is more favorable for SiH_4 insertion than for the three others.

3.3.2. Reaction path properties

The intrinsic reaction coordinate (IRC) calculations on $A + XH_n$ (X = C, Si, P, S; $n = 4, 4, 3, 2$) systems have been performed at the MP2(full)/6-31g(d) level. For instance, Fig. 7 shows the energy changes and the variations of Si–Si*, Si–H*, and Si–F distances along the reaction coordinate in reaction path for $A + SiH_4$ system. The energies and some geometries selected at −14.75, −1.49, 1.49, and 5.99 $(amu)^{1/2}$ bohr along the IRC for SiH_4 insertion are also shown in Fig. 7, where it may be seen that the transition state SiTS3 connects smoothly with the reactants $A + SiH_4$ and the insertion intermediate SiIM1. NBO analysis along this IRC for selected points is given in Table 2. It is obvious that the bond lengths, Si–H* and Si–Si*, change strongly in the course of reaction. The Si–Si* bond rapidly shortens from reactants side and arrives at the equilibrium bond length of SiIM1 at about $s = 1.00$ $(amu)^{1/2}$ bohr. The Si–H* bond arrives at the equilibrium bond length of SiIM1 at about $s = 2.50$ $(amu)^{1/2}$ bohr. It appears that the formation of Si–Si* bond is slightly earlier than that of Si–H* bond. In Table 2 (path III), it is found that the charges of H_2Si moiety increase during the course of reaction with those of H* and H_3Si* decrease, respectively. The occupancies of the lone pair orbital on Si atom (LP_{Si}, σ orbital) are 1.981 and 1.659 at $s = -14.75$ and -0.99 $(amu)^{1/2}$ bohr, respectively, relative to 1.988 in A. Therefore A also shows nucleophilic behaviour in the insertion. In the region from $s = -0.49$ to 5.99 $(amu)^{1/2}$ bohr, the Si–Si* and Si–H* bonds formed with the inversion of configuration of H_3Si*SiH_3 moiety. As a result, the insertion process resembles a S_N2-Si type reaction mechanism [28].

For reactions $A + XH_n$ (X = C, P, and S; $n = 4, 3, 2$), the reaction mechanism are similar to that of $A + SiH_4$ reaction.

3.4. Comparison among three paths

3.4.1. Reaction mechanism

The theoretical results indicate that the insertion reactions of A into X–H bonds proceed via three reaction paths, I, II and III, obtained the same products H_3SiXH_{n-1}. All insertion reactions are exothermic. The schematic diagrams of the potential energy curves at G3(MP2) level are shown in Fig. 8. To obtain a better understanding of the nature of A insertion reaction, a comparison is made among three paths.

Path I and II occur at all seven kinds of X–H bonds. Both two insertion paths involve the initial formation of a precursor complex Xc followed by an intermediate IM via a three-membered ring transition state TS, leading to the product, substituted silane H_3SiXH_{n-1}, with LiF being dissociated apart from the Si atom. The periodic trends for paths I and II are quite similar. For instance, the X–H insertion for the second-row hydrides has a lower activation barrier than that for the first-row hydrides. However, the barrier height of path II is higher than that of path I, correspondingly, i.e., the barrier energy of CTS, NTS, OTS, FTS, and SiTS, PTS, STS

and STS for path II is larger than that for path I by 37.52, 23.67, 19.94, 14.15, and 58.24, 32.68, 16.58 kJ/mol, respectively. The simplest explanation of this barrier difference is that more steric restriction existing in process of path II. As a whole, path I is similar to S_N2-Si type nucleophilic substitution mechanism with the inversion of conformation and path II is similar to S_Ni-Si type nucleophilic substitution mechanism with the retention of conformation. It is reasonable to expect that the product H_3SiXH_{n-1} formed via paths I and II, respectively, would be enantiomorphs if H^1 and H^2 atoms in A were substituted by different atoms or groups. This may help to suggest further synthetic applications.

Path III occurs only at four kinds of X–H (X = C, Si, P, and S) bonds. This path involves the formation of a transition state XTS3, followed by an intermediate XIM1, then to obtain product H_3SiXH_{n-1} with LiF being dissociated apart from the Si atom. As shown in Scheme 1 (2), this insertion pattern is more favorable for A + SiH_4 system. This is due in main part to the electronic effect. As a whole, path III is similar to S_N2-Si type nucleophilic substitution mechanism. In addition, path I is favorable for the insertion reactions of A into CH_4, NH_3, PH_3, H_2O, H_2S and HF.

3.4.2. Bond energy analysis

As seen in Table 1 (MP2(full)/6-31g(d)), it is apparent that the lowest activation barrier in three paths in the order: CH_4 (241.73 kJ/mol) > NH_3 (170.09 kJ/mol) > H_2O (110.43 kJ/mol) > HF (53.52 kJ/mol) and PH_3 (117.23 kJ/mol) > SiH_4 (96.22 kJ/mol) > H_2S (84.50 kJ/mol). In addition, the barrier heights for the first-row hydrides are much higher than those for the second-row hydrides. Furthermore, the reaction enthalpy for these XH_n hydrides increases in the order: CH_4 (−5.09 kJ/mol) > NH_3 (−62.69 kJ/mol) > H_2O (−113.22 kJ/mol) > HF (−177.27 kJ/mol) and SiH_4 (−17.96 kJ/mol) > PH_3 (−36.67 kJ/mol) > H_2S (−75.52 kJ/mol). Since the reactions involve the breaking of X–H bonds and making of Si–H and Si–X bonds, the strength of them becomes an important consideration. Bond energy is a measure of bond strength, which is the energy required to break a covalent bond homolytically (into neutral fragments). Table 3 is a collection of bond energies for X–H bonds in XH_n molecules and Si–X bonds in H_3SiXH_{n-1} molecules at MP2(full)/6-31g(d) level. Some useful and interesting conclusions may be drawn from this table. First, the X–H bond strengths for the first- and second-row hydrides increase, respectively, in the order of N–H < C–H < O–H < F–H and P–H < S–H < Si–H. It seems for A insertion the F–H bond is more difficult to activate than the other three bonds of the first-row hydrides. However, the Si–X bond strengths in H_3SiXH_{n-1} molecules increase in the order of Si–C < Si–N < Si–O < Si–F and Si–P < Si–Si < Si–S. Therefore the Si–F bond is the strongest one in the first-row products molecules H_3SiXH_{n-1}. As a result, the reaction with HF molecule occurs easiest. The same situation can also be found in the second-row hydrides as shown earlier. Second, for the same family systems, the X–H bond strength for the first-row hydride is bigger that that for the corresponding second-row hydride. Namely, the C–H bond is more difficult to activate than the Si–H bond. Therefore, the X–H insertion for the second-row hydrides has a lower activation barrier than that for the first-row hydrides. Third, from Table 3, the results suggest a increasing trend in ΔE for $CH_4 < NH_3 < H_2O <$ HF and $SiH_4 < PH_3 < H_2S$, which is in agreement with the trend in the enthalpy for A insertion as shown above. Consequently, on the basis of the present computational results, we predict that the reactivity of XH_n hydrides toward the p-complex structure A increases in the order C < N < O < F and P < Si < S. The reactivity of the second-row hydrides is higher than that of the first-row ones.

Table 3
The calculated bond energies (kJ/mol) of X–H bonds in XH_n molecules and Si–X bonds in H_3SiXH_{n-1} molecules at MP2(full)/6–31g(d) level

E_{X-H}[a]		E_{Si-X}[b]		ΔE[c]	
F–H	516.93	Si–F	629.87	CH_4	112.94
O–H	466.83	Si–O	515.71	H_2O	48.88
N–H	434.26	Si–N	432.61	NH_3	−1.65
C–H	435.25	Si–C	376.00	CH_4	−59.25
S–H	337.06	Si–S	348.24	H_2S	11.18
P–H	310.43	Si–P	282.76	PH_3	−27.67
Si–H	353.03	Si–Si	306.64	SiH_4	−46.39

[a] $E_{X-H} = E_{H_{n-1}X} - E_{XH_n}$.
[b] $E_{Si-X} = E_{H_3Si} + E_{H_{n-1}X} - E_{H_3SiXH_{n-1}}$.
[c] $\Delta E = E_{Si-X} - E_{X-H}$.

4. Concluding remarks

In the present work, we have studied the reaction mechanisms of the p-complex structure (A) of silylenoid H_2SiLiF insertion into the X–H bond of the first- and second-row XH_n molecules by G3(MP2) theory. Three reaction paths, I, II and III, were obtained. It should be pointed out that this study has provided the first theoretical demonstration about the reaction trajectory and theoretical estimation of the activation energy and reaction enthalpy for those processes.

1. The theoretical results suggest that A inserts a X–H bond in a concerted manner via a three-center-type transition state, and that the stereochemistry at the heteroatom X center is preserved.
2. From both a kinetic and thermodynamic viewpoint, for X–H bonds the order of reactivity by A insertion via path I and II is F > O > N > C and S > P > Si; that via path III is Si > P > S > C. These results can be easily understood in terms of electronic and steric effects.
3. Paths I and III are similar to S_N2-Si type nucleophilic substitution mechanism with the inversion of conformation and path II is similar to S_Ni-Si type nucleophilic substitution mechanism with the retention of conformation.

4. Path I is favorable for the insertion reactions of A into CH_4, NH_3, PH_3, H_2O, H_2S and HF, and path III is favorable for $A + SiH_4$ system.
5. The reactivity of XH_n hydrides toward A increases in the order $C < N < O < F$ and $P < Si < S$. The reactivity of the second-row hydrides is higher than that of the first-row ones.

Furthermore, because of a lack of experimental data on such insertion reactions, our conclusions above may be considered as predictions for future investigation.

Acknowledgements

This work was supported financially by the National Nature Science Foundation of China (No. 20373034), PhD Special Research Foundation of Chinese Education Department, and High Performance Computational Center of Shandong University.

Appendix A. Supplementary data

Supplementary data associated with this article can be found, in the online version, at doi:10.1016/j.jorganchem.2005.08.031.

References

[1] H. Gilman, D.J. Peterson, J. Am. Chem. Soc. 87 (1965) 2389.
[2] O.M. Nefedow, M.N. Manakow, Angew. Chem. 76 (1964) 270.
[3] C.L. Smith, R. Gooden, J. Organomet. Chem. 81 (1974) 33.
[4] R. West, J. Organomet. Chem. 300 (1986) 327.
[5] P. Boudjouk, U. Samaraweera, R. Sooriyakumaran, J. Chrusciel, K.R. Anderson, Angew. Chem. Int. Ed. Engl. 27 (1988) 1355.
[6] T. Tsumuragua, S.A. Batcheller, S. Masamune, Angew. Chem. Int. Ed. Engl. 30 (1991) 902.
[7] T. Tsumuragua, S.A. Batcheller, S. Masamune, Angew. Chem. 103 (1991) 916.
[8] K. Tamao, A. Kawachi, Y Ito, J. Am. Chem. Soc. 114 (1992) 3989.
[9] R. Corriu, G. Lanneau, C. Priou, F. Soulairol, N. Auner, R. Probst, R. Conlin, C.J. Tan, J. Organomet. Chem. 466 (1994) 55.
[10] A. Kawachi, K. Tamao, Organometallics 15 (1996) 4653.
[11] A. Kawachi, N. Doi, K. Tamao, J. Am. Chem. Soc. 119 (1997) 233.
[12] K. Tamao, A. Kawachi, Angew. Chem. Int. Ed. Engl. 34 (1995) 818.
[13] Y. Tanaka, A. Kawachi, M. Hada, H. Nakatsuji, K. Tamao, Organometallics 17 (1998) 4573–4577.
[14] Myong Euy Lee, Hyeon Mo Cho, Young Mook Lim, Jin Kyong Choi, Chang Hee Park, Seong Eun Jeong, Uk Lee, Chem. Eur. J. 10 (2004) 377.
[15] T. Clark, P.R. Schleyer, J. Organomet. Chem. 191 (1980) 347.
[16] S.Y. Feng, G.Z. Ju, C.H. Deng, Chem. Phys. Lett. 186 (1991) 248.
[17] S.Y. Feng, D.C. Feng, C.H. Deng, Chem. Phys. Lett. 214 (1993) 97.
[18] S.Y. Feng, D.C. Feng, J.H. Li, Chem. Phys. Lett. 316 (2000) 146.
[19] S.Y. Feng, D.C. Feng, J. Mol. Struct. (Theochem.) 541 (2001) 171.
[20] S.Y. Feng, Y.F. Zhou, D.C. Feng, J. Phys. Chem. (A) 107 (2003) 4116.
[21] D.C. Feng, J. Xie, S.Y. Feng, Chem. Phys. Lett. 396 (2004) 245.
[22] L.A. Curtiss, P.c. Redfern, K. Raghavachari, V. Rassolov, J.A. Pople, J. Chem. Phys. 110 (1999) 4703.
[23] C. Gonzalez, H.B. Schlegel, J. Chem. Phys. 90 (1989) 2154.
[24] C. Gonzalez, H.B. Schlegel, J. Phys. Chem. 94 (1990) 5523.
[25] J.P. Foster, F. Weinhold, J. Am. Chem. Soc. 102 (1980) 7211–7218; A.E. Reed, F. Weinhold, J. Chem. Phys. 78 (1983) 4066–4073; F. Weinhold, Natural bond orbital methods, in: P.v.R. Schleyer (Ed.), Encyclopedia of Computational Chemistry, vol. 3, 1998, pp. 1792–1811.
[26] M.J. Frisch, et al., Gaussian, Inc., Pittsburgh PA, 2003.
[27] G.S. Hammond, J. Am. Chem. Soc. 77 (1954) 334.
[28] L.H. Sommer, C.M. Golino, D.N. Roark, R.D. Bush, J. Organomet. Chem. 49 (1) (1973) C3–C5.